The Cryosphere Discuss., 8, 6117–6146, 2014
www.the-cryosphere-discuss.net/8/6117/2014/
doi:10.5194/tcd-8-6117-2014

The Cryosphere Discussions
Open Access

Role of rainwater induced subsurface flow in water-level dynamics and thermoerosion of shallow thermokarst ponds on the Northeastern Qinghai–Tibet Plateau

X. Pan[1,2], Q. Yu[1], and Y. You[1]

[1]Laboratory of Frozen Soils Engineering Cold and Arid Regions Environmental and Engineering Research Institute, CAS, Lanzhou, China
[2]Global Institute for Water Security, University of Saskatchewan, Saskatchewan, Canada

Received: 25 October 2014 – Accepted: 24 November 2014 – Published: 11 December 2014

Correspondence to: Q. Yu (yuqh@lzb.ac.cn)

Published by Copernicus Publications on behalf of the European Geosciences Union.

Abstract

Understanding hydrological and thermal regimes of thermokarst lakes is of great importance for predicting their responses to climate change. However, mechanism of water-level dynamics and associated thermal effects on thermoerosion of thermokarst lakes are still not well understood on the Qinghai–Tibet Plateau (QTP). In this study, we investigate two typical shallow thermokarst ponds (namely small lakes) in a warm permafrost region with thick active layer on the northeastern QTP through quantifying water budget. Results demonstrate that, rainfall induced subsurface lateral flow dominates pond water-level regime. Annual variation of pond water-level relies on areal water budget of surrounding active layer, particularly the high variable of precipitation. Besides, it is worth noting the extraordinary warming during the late ice-cover period, because marked air gap between upper ice-cover and underlying water, led by the upward thawing of thick ice-cover, might result in greenhouse-like condition due to the unique weather that strong solar radiation and little snowpack. This hydrological mechanism also exerts evident impacts on thermal regime and thermoerosion of the shallow thermokarst ponds, and they are closely related to retreat of thermokarst pond-shore and underlying permafrost degradation. These findings imply a localized model addressing the unique hydrological and thermal regimes of thermokarst lakes would be essential to study the evolution of these shallow rainwater dominated thermokarst ponds on the QTP.

1 Introduction

Thermokarst lakes are typically formed by the settlement of ground following thawing of ice-rich permafrost or melting of massive ice (van Everdingen, 1998). They are usually located at permafrost-dominated lowland regions with high to moderate ground ice content (Grosse et al., 2013). Thermokarst lakes are widely distributed throughout pan-Arctic lowlands, and a total area of 414 400 km^2 were found in permafrost

regions north at 45.51 latitude excluding Greenland (Smith et al., 2007). The lake area fraction exceeds 40 % in some of the thermokarst-affected lowland regions, such as the Northeast Siberian coastal lowlands, northern West Siberia, Alaska North Slope, Yukon–Kuskokwim Delta region, and Mackenzie Delta region (Grosse et al., 2013). However, thermokarst lakes also appear in the alpine permafrost (e.g. Kääb and Haeberli, 2001; Harris, 2002; Lin et al., 2010), but there are sparsely distributed. On the Qinghai–Tibet Plateau (QTP), investigation of thermokarst lakes in a representative region along the Qinghai–Tibet corridor from Kunlun Mountain to Fenghuo Mountain pass along the Qinghai–Tibet Railway by Niu et al. (2011) shows that comparably high lake area fraction only appear in relatively flat area like Chumaer High Plain, while it is very low in mountainous areas like the Kunlun Mountains region and the Fenghuo Mountains region.

Water-level dynamics of lakes are controlled by the balance between inputs and outputs of water, which are strongly influenced by the hydrological processes (Hayashi and van der Kamp, 2007). Particularly, many hydrological processes in permafrost regions are sensitive to climate change, as well as related permafrost aggradation or degradation. Changes in thermokarst lakes due to climate warming and permafrost degradation have been reported in the Arctic and QTP (Smith et al., 2005; AMAP, 2011). For instance, gradual and catastrophic changes in lake morphology are found to be strongly related to hydrologic variability of thermokarst lakes (Hinkel et al., 2007; Pohl et al., 2007; Marsh et al., 2009; Turner et al., 2010). Given a common mechanism of near-surface flow through the troughs of ice wedge polygons and subsurface flow of water through thermal contraction cracks in inter-connected ice wedges (Mackay, 1992), the study of a thermokarst lake in the Mackenzie Delta region, Canada (Pohl et al., 2009) shows that the lake drainage is usually initiated during periods of high lake water levels in the spring snowmelt runoff period or after periods of heavy rainfalls during the summer. Spring snowmelt recharge commonly represents the dominant flux in the thermokarst lake water balance in the Arctic and sub-Arctic. However, the summer rainfall is the major input for the thermokarst lakes on the QTP, and the snowfall is

rather small. In addition, permafrost on the QTP is characterized as thick active layer. Therefore, unique hydrological regime is expected on the QTP.

The development of thermokarst lakes is not only controlled by its thermal regime but also hydrological regime. Due to the unique geography of the QTP, its climate is characterized as cold and dry, and its precipitation is mainly controlled by the summer monsoon (Ma et al., 2006). However, features of thermokarst lakes and their responses to the climate change are rarely reported till recent years. A general investigation of thermokarst lakes along part of the Qinghai–Tibet Railway from a high-resolution map (Niu et al., 2011) shows that denser lakes lying on the Chumaer High Plateau than the other mountainous regions and most of them are shallow that it would be frozen to lake bottom in winter. Besides, most of the lakes are elliptical or elongated. Thermal regime of an individual lake in the Beiluhe Basin by Lin et al. (2010) demonstrates that the 2 m deep lake was not frozen at bottom and strong lateral erosion occurred as the lake edge retreated as much as 1.8 m from 2007 to 2008. This thermokarst lake is turned out to be an open talik from deep borehole temperature measurements (Niu et al., 2011). Observations of lake-bottom temperature from a variety of thermokarst lakes in Chumaer High Plain, Hoh Xil Hill Region and Beiluhe Basin (Niu et al., 2011) demonstrate that lake thermal regimes are strongly related to water depth. However, few studies of hydrological regime have been reported for the shallow thermokarst lakes in the other regions so far, and the mechanism of thermokarst lake water-level dynamics and its impact on thermal regime are still not well understood.

Understanding the seasonal and the long-term hydrologic behaviour of thermokarst lakes are of great importance for predicting changes of thermokarst lakes on the QTP. Based on limited hydro-climatological observations, we explored the hydrological features of shallow thermokarst ponds in a continuous permafrost region on the northeastern QTP. The objective of this study are: (1) to characterize the water budget of two different shallow thermokarst ponds; (2) to identify the controlling factors of the pond water-level dynamics; (3) to reveal the relation between hydrological regime and pond thermoerosion.

2 Site description

The study site is located at 35°11′ N, 93°57′ E with an elevation of 4445 m a.s.l. in the north-eastern QTP, China (Fig. 1). It lies on the riverbank of the Chumaer River on the Chumaer High Plain. The terrain is gently declining to the river, and a large amount of small and shallow thermokarst ponds spread in this region (Niu et al., 2011). The ground mainly consists of a thin top soil of quaternary sandy loam, a non-uniform alluvial gravel layer and a thick underlying tertiary mudstone.

The record of meteorological data from 2007 to 2011 (Pan et al., 2014) shows that, the mean annual air temperature was −4.0 °C and the mean annual precipitation was about 300 mm. Observations from the weather stations (Li et al., 2006) shows only 2.3 % of precipitation occurred as snow in winter from 1962 to 2004 in this region. The summer monsoon-driven precipitation mainly concentrates from June to September, and temporal thin snow cover usually appears pre- and post of the rainy season. Permafrost in this area consists of a thick active layer (> 2 m) and underlying ice-rich permafrost with a thickness of 20–30 m (Zhou et al., 2000).

Two thermokarst ponds (Pond 1 and Pond 2, Fig. 1b), a few kilometers from the Chumaer River, were selected to investigate their hydrological regimes. Both of them are in a rectangular shape, and the deep parts orientate to the river in the north. The open-water areas of Pond 1 and Pond 2 are about 50 m × 120 m and 70 m × 220 m, respectively. Pond 1 is relative isolated to other ponds, while Pond 2 is connected to the other ponds via a flow trail (dashed line in Fig. 1b).

3 Material and methods

3.1 Instrumentation

A soil–weather monitoring station is located in between the two ponds (Fig. 1b). Regular meteorological measurements including air temperature, relative humidity, wind

speed and direction, net radiation, precipitation and subsurface soil measurements (soil temperature and soil water content) were collected hourly using a datalogger. Air temperature and relative humidity were measured at 2.0 m a.g.l. Net radiation was measured 1.5 m a.g.l. Wind speed and direction were measured 2.0 m a.g.l. Rain Gauge (RM Young 52202; Campbell Scientific, Logan, UT) was used to measure rainfall, while the solid precipitation was simply diagnosed by measuring the snow depth using an Ultrasonic Distance Sensor (SR50; Campbell Scientific, Logan, UT). Under the ground, one soil pit was excavated until frozen ground was encountered in the late summer of 2006. Soil temperature was measured at depths of 0.05, 0.10, 0.15, 0.20, 0.30, 0.50, 0.70, 0.90, 1.10, 1.30, 1.50, 1.70, 1.92, 2.08, 2.18, 2.30, 2.50, 2.70, 3.00, 3.30, 3.60 m using a combined soil temperature probes: model 107 (Campbell Scientific, Logan, UT) and calibrated thermistor probes (State Key Laboratory of Frozen Soil Engineering, CAS), respectively. Soil water content was measured at depths of 0.10, 0.20, 0.40, 0.65, 0.89, 1.19, 1.535, 1.92, 2.10 m using CS616 (Campbell Scientific, Logan, UT). The ice content was calculated using the pre-freeze soil water content minus the measured unfrozen water content.

The talik dimension of Pond 1 was characterized using three boreholes (B1, B2 and B3 in Fig. 1c). Borehole temperatures of the former two were measured using a series of calibrated thermistor probes on 26 May 2014, and the latter one was measured with the same method on 20 February 2014. Permafrost base was determined as the depth with a temperature of 0 °C. For comparison, ground temperature from the fourth borehole located at a few hundred meters away from the pond 1 (B4 in Fig. 1b) was measured on 20 February 2014.

Pond water level and bottom temperature dynamics at the two ponds were monitored using two water-level loggers (HOBO U20 Water Level Data Logger, Onset Computer Corporation) with an accuracy of 5 mm in water-level and 0.44 °C in temperature. They were put at the pond bottom about one meter blow water surface. The water-level logger at Pond 1 was reset as measuring every two hours since 26 October 2013.

3.2 Estimating pond evaporation

For estimating evaporation from a shallow water body, there are a wide variety of methods reported in the literature and used in practice (e.g. Finch and Calver, 2008). Particularly, the combination of the aerodynamic and energy balance procedures is desirable. Based on measurements from the automatic weather station nearby the ponds, evaporation from open water E can be determined using the reference evapotranspiration ET_0 with a coefficient K_w as follows

$$E = K_w ET_0. \tag{1}$$

As suggested by FAO-56 (Allen et al., 1998), a value of 1.05 is given to K_w for the shallow pond with a depth of less than 2 m. The reference evapotranspiration ET_0 mm d^{-1} for short grass is calculated using the Penman–Monteith method (Allen et al., 1998). The equation is

$$ET_0 = \frac{0.408\Delta(R_n - G) + \gamma \frac{900}{T_a+273} u_2 (e_s - e_a)}{\Delta + \gamma(1 + 0.34u_2)} \tag{2}$$

where: R_n: net radiation, MJ m^{-2} d^{-1}; G: soil heat flux density, MJ m^{-2} d^{-1}; T_a: mean daily air temperature, °C; u_2: mean daily wind speed at 2 m height, m s^{-1}; e_s and e_a: saturated and actual vapor pressure, respectively, kPa; Δ: slope vapor pressure curve, kPa °C^{-1}; γ: psychometric constant, kPa °C^{-1}.

Soil heat flux density G in Eq. (2) is determined by measuring the total thermal energy change in the active layer. The total energy including sensible heat and latent heat can be calculated from soil temperature and water content measurements in the active layer. Here an areal density E_t is used to present the stored energy in the active layer from the surface to a reference depth z_r m, and it is calculated with respect to the

reference state where the soil ideally contains only soil matrix at a temperature of zero.

$$E_t(t) = \sum_{\alpha \in \{s,w,i\}} c_\alpha \rho_\alpha \int_0^{z_r} \theta_\alpha(z,t) T(z,t) \mathrm{d}z - L_{sf} \rho_i \int_0^{z_r} \theta_i(z,t) \mathrm{d}z \tag{3}$$

where: s, w, i: indices of soil matrix, unfrozen water and ice, c_α: specific heat of the materials, MJ kg^{-1} K^{-1}; ρ_α: density of the materials, kg m^{-3}; L_{sf}: latent heat of fusion from solid to fluid, MJ kg^{-1}; θ_α: volumetric content of each phases, m^3 m^{-3}.

Given a deep reference depth with negligible heat flux below it, surface soil heat flux density G is approximately calculated as

$$G(t) = \frac{\partial E_t(t)}{\partial t}. \tag{4}$$

Saturated vapor pressure in Eq. (2) is calculated by averaging the saturated vapor pressure at daily extremes of air temperature (T_{max}, T_{min}) as

$$e_s = \frac{e_{(T_{max})} + e_{(T_{min})}}{2} \tag{5}$$

where $e_{(T_{max})}$ and $e_{(T_{min})}$ are calculated using the formula

$$e_T = 0.6108 \exp\left(\frac{17.27 T_a}{T_a + 237.3}\right). \tag{6}$$

Actual vapor pressure is calculated with measured relative humidity

$$e_a = \frac{RH_{mean}}{100} \exp\left(\frac{e_{(T_{max})} + e_{(T_{min})}}{2}\right). \tag{7}$$

3.3 Rainfall estimation through soil water content observations

Since maintenance of the auto-weather station in the remote and harsh field is difficult, the rain gauge sometimes did not work properly. Correction is required for the rainfall measurements. A robust method of estimating precipitation rate proposed by Brocca et al. (2013) was used in this study. It is briefly introduced here, and more detail can be found in that paper. This approach bases on a simplified water balance for a shallow layer depth, where precipitation, fluctuation rate of soil water storage and drainage rate are included, while other processes like evaporation, runoff are neglected. This assumption is reasonable for our study site, where overland flow is not expected due to the flat surface at the measurement location and large capacity of sandy loam soil. The equation is given as

$$p(t) \approx Z\frac{\partial s(t)}{\partial t} + as(t)^b, \tag{8}$$

where Z is the soil layer thickness, $s(t)$ is the relative saturation of the soil, t is the time, a and b are the parameters of the drainage rate. The second term is adopted from the relation by Famiglietti and Wood (1994). The parameters (Z, a and b) could be estimated through calibration, and the discrete form of Eq. (8) is solved by using a fourth-order Runge–Kutta scheme.

3.4 Determining net lateral water flux

Water level changes in ponds and lakes are controlled by the balance between inputs and outputs of water. The inputs at the studied ponds mainly include precipitation, and surface–subsurface lateral inflow, and the outputs include evaporation and surface–subsurface lateral outflow. Water balance of the ponds is generally expressed as

$$P - E + \Delta L = \Delta S \tag{9}$$

where, P: precipitation (including solid and fluid forms), $\mathrm{mm\,d^{-1}}$; E: actual evaporation, $\mathrm{mm\,d^{-1}}$; ΔL: net lateral water flux, which equals the difference between inflow and

outflow by surface runoff and subsurface flow in the saturated zone over thawing table, $\mathrm{mm\,d^{-1}}$; ΔS: the talik water storage change, $\mathrm{mm\,d^{-1}}$.

Precipitation in the studied region is dominated by the summer-monsoon, and solid precipitation is less that 10 % of the annual total precipitation. Therefore, only the estimated rainfall during ice-free period was used in this study. The talik water storage change was determined from the measured water level. Since the dense weathered mudstone with high clay content indicates a low hydraulic conductivity, the percolation is thought to be negligible here. The pond evaporation E is calculated with the above mentioned method (Eq. 1). Since the net lateral water flux ΔL include surface runoff and subsurface flow in the saturated or near saturated thawed soils in the active layer, it is difficult to measure separately. Particularly, preferential subsurface flow above the uneven thawing table further complicates the measurements. In this study, ΔL is determined using Eq. (9) by assuming closure of water balance.

For the ice-cover period, evaporation and precipitation become negligible in Eq. (9). Thus, change in pond water storage including ice-cover and underlying liquid water is mainly related to subsurface water flow before completely frozen of surrounding active layer. So the total net lateral flux during ice-cover period could be deduced from the difference in water-level between pre-freezing and post thawing of ice-cover.

4 Results

4.1 Hydrological conditions of the shallow thermokarst ponds

Except precipitation and evaporation, water balance of a lake could be influenced by surface runoff, and subsurface groundwater flow. Since the studied ponds are located at permafrost area, subsurface lateral flow above the thawing table surrounding the lake edge may recharge the ponds. Subsurface lateral flow is thought to happen at both ponds when the thawing front is lower than the groundwater table. However, surface runoff might only occur at Pond 2 when meeting heavy rainfall or snowmelt in spring.

In addition, pond water might be lost by subsurface seepage, but this depends on the thermal structure of the talik and the hydrogeological condition.

The positive ground temperature measured in late May in 2014 indicates that Pond 1 is an open talik, which means no permafrost underneath the pond. Since pond water depth is a key factor to the pond water regime, Pond 2 with deeper water is thought to be likely also an open talik. However, the areal strata consisted of surficial diluvium of the Quaternary Holocene Series and underlying thick lacustrine deposits of the upper Tertiary, and the permeability of the lower layer is usually extremely low. Drilling of the boreholes (Fig. 1b and c) show that the thickness of the surficial layer of sandy loam and gravel surrounding the ponds is 2–2.5 m, and the thickness of the underlying weathered mudstone is over 20 m. Therefore, subsurface groundwater percolation would be negligible at both ponds.

4.2 Rainfall estimation through soil water content measurements

Rainfall estimation is carried out by using hourly in-situ soil water content measurements at depths of 10, 20 and 40 cm, where the soil texture is sandy loam with a mean porosity of 0.4. The calibration was conducted by using data from 29 June to 3 November in 2012 (gray area in Fig. 2a) and afterward estimation was calculated using the calibrated parameters. The observed and calibrated daily rainfall data match well, but distinct differences occurred in 2013. The evident difference during the period from 10 July to 6 August in 2013 in the upper plot are likely due to the malfunction of the rain gauge, while underestimation during the maximum peak indicates slight surface runoff might happen because of the heavy rainfall. However, considering large uncertain of the observed rainfall data, the estimated rainfall is more reliable. All the following analyses are based on the estimated rainfall.

4.3 Characteristics of pond water-level dynamics

Pond water level is influenced by the seasonal and inter-annual variability of the inputs and outputs. They mainly include precipitation, evaporation, surface and subsurface lateral flow. Since pond water-level and associated processes differed significantly between ice-free period and ice-cover period, they are analyzed separately in the following. According to field observations of ice formation by Niu et al. (2011), the ice-cover period in this region starts from the middle of October to the middle of May in next year. But the specific ice-cover periods at the studied ponds (gray areas in Fig. 3b) were deduced according to the features of measured pond bottom temperature and their relation with pond water depth. First, since presence of ice-cover turns energy exchange at water surface from convective heat transfer to heat conduction, the daily amplitude of pond bottom temperature fluctuation would be reduced. Second, the temperature differences at two ponds can further consolidate the deduction of ice-cover period (Fig. 6). Since the temperature difference is controlled by water depth when conductive heat transfer dominates pond thermal regime below the ice-cover, while the strong surface convective heat transfer can weaken the effect of water depth difference, and make the bottom temperature difference rather small.

The dramatic changes in pond water level during the ice-free periods in Fig. 3b are strongly related to the rainfall. Since the rainy season usually starts from June to September in the northeastern QTP, three sub-periods with different features of water level can be summarized. Before the rainy season the influence of active layer thawing on the pond water-level was negligible till the thawing front reached the saturated zone at a depth of about 1.2 m, because the upper part of the active layer was dry (Fig. 3c). Therefore, pond water-level dropped slightly due to prevalent evaporation during this sub-period (Fig. 3b). During the rainy season evident pond-water jumps occurred with intensive rainfall events. There was only one evident jump after June in 2012, but three clear jumps occurred in 2013. This is likely related to the rainfall intensity and duration. Since the intensive rainfall events could quickly reach the saturated layer (here-

after we call is groundwater for short), whereas small rainfall would be overwhelmingly lost by evapotranspiration from near-surface soils, and little rainwater can contribute to groundwater. This is further corroborated by soil water content measurements in Fig. 3c. Above the water table the unsaturated layer is about 1.2 m thick. The wetting necks between the top soil and bottom saturated soils imply the recharges of rainfall to the water table. Therefore, the response of pond-water level was not significant when the rainfall were too small to recharge groundwater. During the post rainy season, pond water-level did not show significant increase but slightly decrease although active layer was still thickening. This implicates that compared to the contribution of the intensive rainfall events it is much weaker for the deepening of thawed layer to contribute the lake water storage.

Pond water level dropped evidently through the ice-cover periods (grey areas) in Fig. 3b. Before completely frozen to bottom, the declining water-level could be led by groundwater flow through the unfrozen layer. Since pond water was connected with groundwater and also atmosphere through the unsaturated active layer, the measured water level includes the pressure of upper thickening ice layer till the active layer was completely frozen. The following measured extreme values, not shown in Fig. 3b, were caused by the freezing of the compressed pond water and bottom soil. Afterward there is not too significant change in water-level when pond bottom started thawing. The total drop of water-level before and after the ice-cover period 1 reached 406 and 323 mm at Pond 1 and Pond 2, respectively. During the ice-cover period 2, the drops at both ponds were smaller, but the drop at Pond 2 was still bigger than that at Pond 1.

4.4 Significant role of rainwater induced subsurface lateral flow in pond water-level regime

Water budget of the thermokarst ponds was calculated for the ice-cover period and the ice-free period separately. Since surface water exchange was nearly locked during the ice-cover period, precipitation and evaporation were close zero. Majority of the water loss (Fig. 3b) is attributed to subsurface lateral flow. However, the role of subsurface

lateral flow is more complex during ice-free period. Particularly for Pond 2, surface runoff through the trail might also contribute to the pond water budget. For instance, the water-level jumps in Fig. 3b are quite similar at both ponds in the summer of 2012, while the water-level jumps at the Pond 1 are much bigger that those at Pond 2 in the summer of 2013. The difference in water-level jump at the two ponds is likely to be related to the closure of pond water. Besides, sharp peaks occurred at Pond 2 when meeting intensive rainfall events but there was not evident recession at Pond 1. This further consolidated that Pond 2 can interact with temporal stream runoff.

Figure 4 shows the feature of water budget during ice-free periods at the two ponds in 2012 and 2013. Generally, three sub-periods are summarized as follows. (1) During the pre-rainy season, pond water-level regime was dominated by evaporation, and the net lateral flux started active when the thawing front in surrounding active layer reached precedent water-level. Duration of this sub-period depends on start timing of the rainy season in different years. (2) During the rainy season, the pond water-level regime was strongly correlated with the rainfall induced net lateral flux. For instance, the jumps or peaks are always coincident with heavy rainfall events. The jumps would be caused by continually positive net lateral flux when pond water-level was lower than surrounding groundwater level, while the peaks would attribute to recharge and discharge by stream runoff when pond water-level was higher than surrounding groundwater level. (3) During the post rainy season, the pond water-level regime was controlled by the prevalent evaporation and the elevation difference between pond water-level and surrounding groundwater level.

Since the interaction between pond water and surrounding groundwater is influenced by surface runoff, the role of net lateral flow at the two ponds differs slightly. The comparison of net lateral flux at two ponds in 2012 and 2013 is shown in Fig. 5. Pond 1 is water closed without stream inflow and outflow, while Pond 2 is temporally open to the streams. Therefore, sharp peaks of net lateral flux occurred at Pond 2 during heavy rainfall (Fig. 5), while it is not evident at Pond 1. Except the pond type, topography also influences the interaction between pond water and surrounding groundwater. For

instance, the accumulative net lateral flux became negative at the end of 2012, while it was about 184 mm at Pond 2. In contrary, the accumulative net lateral flux was much bigger at Pond 1 than at Pond 2 in 2013, and the latter one was quite similar in 2012 and 2013. The yearly contrast change of accumulative net lateral flux at Pond 1 would be attributed to the imbalance between groundwater inflow and outflow. Since Pond 1 is located at an evident declining area, groundwater inflow would decline from the upper land in the late autumn, but the outflow would steadily increase at the low land along with deepening thawing front. But in the wet year of 2013, sufficient groundwater inflow from the upper land with high hydraulic gradient exceeded the outflow at the low land. Therefore, net lateral flux continuously increased except the period from the end of July to the end of August with deficit between precipitation and evaporation. In contrary, Pond 2 is located at the rather flat area, the groundwater inflow and outflow would be comparable when pond water-level equals the groundwater level. This further consolidated the deduction that groundwater in surrounding active layer strongly influences the pond water-level.

In general, annual fluctuation of pond water-level at the study site is mainly controlled by rainfall, but for specific ponds it can be modified due to the influence of micro-topography on the interaction between pond water and areal groundwater in active layer. Being different from the hydrological regime in Arctic (Bowling et al., 2003; Pohl et al., 2007), spring snowmelt and active layer thawing are not significant in the studied region. Given dry and thick active layer, overland flow during rainfall is not expected, but subsurface lateral flow in surrounding active layer plays an important role in pond water-level dynamics in the studied region. The areal water-level in active layer mainly relies on the areal water budget between precipitation and evaporation. Without significant contribution of subsurface lateral flow this kind of shallow thermokarst ponds could dry out due to the high potential evaporation.

4.5 Thermal impacts of hydrological regime on shallow thermokarst ponds

The above hydrological regime can exert significant thermal impacts on thermoerosion of the shallow thermokarst ponds. A previous study of Pond 1 by Pan et al. (2014) demonstrates that the preferential lateral flow can even influence the shape and future development of the thermokarst pond. For instance, the two bulges in the lake shape (arrows in Fig. 1c) are consistent with the inlets of preferential flow paths, which indicate the influence of preferential flow on lake-edge formation. In addition, the rain driven annual fluctuation of areal groundwater level, as well as pond water-level can also lead significant thermal impacts on the thermal regime of these shallow thermokarst ponds. For instance, the freezing degree-day at pond bottom in 2013 (Fig. 6a) was much smaller than that in 2012 at Pond 1 due to the contrast water-level difference during the ice-cover period. However, the freezing degree-days were quite similar at Pond 2 because of the rather stable water-level.

More details about the thermal impacts of seasonal fluctuation of water level are discussed separately in ice-free period and ice-cover period. During ice-free period, the rainwater-induced fluctuation led significant difference in water depth (D_1 and D_2) at Pond 1 and Pond 2 (Fig. 6b), but the difference in pond bottom temperature (T_1 and T_2) is rather small and noisy. This is likely due to the strong wind-induced convective heat exchange in shallow water and lateral groundwater input. However, the difference in water-level would influence the pond bottom thermal regime during subsequent period. Once ice started covering the ponds, the difference between T_1 and T_2 varied greatly in daily fluctuation. During the first ice-cover period, T_1 was smaller than T_2 except the beginning, and prominent difference occurred since the end of February till late April. But during the second ice-cover period T_1 was larger than T_2 till later February, then there was also a prominent increase of temperature difference between T_1 and T_2. The flip of temperature difference in the first half period between Pond 1 and Pond 2 in two ice-cover periods is mainly related to the water depth. Since the ice-cover was thickening from surface to bottom during first half of ice-cover period, the bottom temperature

would be warmer when it is deeper. Whereas, the similar dramatic increase of temperature difference between T_1 and T_2 at the second half of two ice-cover periods would be attributed to the subsurface lateral flow during downward freezing and subsequent upward thawing. During the downward freezing, the pond water can still drain by subsurface lateral flow. As a result, the pond water-level was smaller than that pre-freezing (Fig. 6b), although the decrease of water-level was slight contributed by evaporation during thawing. During the subsequent period with downward and upward thawing, the transformation from ice to water might lead air gap between ice-cover and underlying water, which can significantly change the heat transfer. As a result, significant warming might happen, because the relatively closed air gap can lead green-house effect when the ice-cover is transparent enough. The observed extraordinary high bottom temperature (dashed black and red boxes in Fig. 6) during the thawing periods is consistent with our deduction. The warming effect is particularly prominent at Pond 2, because it thawed much earlier than that at Pond 1. In addition, the deduction is further consolidated by and the similar pond bottom temperature at both ponds once after ice-cover disappearance, as well as the whole ice-free periods.

Thermoerosion of thermokarst ponds in depth is straightforward, but its lateral thermoerosion can also interact with pond water-level dynamics. The impact of lateral thermoerosion of the pond is analyzed by comparing the ground temperature at natural condition without influences of ponds. Thermal structure of the pond 1 can be approximately delineated by using the borehole temperature measurements in Fig. 7. The positive temperature gradient below 8 m at the location of B2 (Fig. 7b) indicates that the pond is still warming the underground. However, ground temperature measured at the pond edge B1 and B3 (Fig. 7a and c) show that a layer of 20 m thick permafrost still exists, although they are just a few meters away from the pond edge. Compared to the shallow ground temperature (< -14 m) measured at B4 (Fig. 7c), the ground was even colder at the pondshore, particularly at B3. This might be attributed to local soil water dynamics that impacts ground heat transfer. From the above analysis of the pond water-level dynamics, we recall that soil water at the pondshore increased due to

elevated lake water-level in rainy season, and decreased notably due to pond water depletion by subsurface flow before freezing. Compared to natural ground, for instance at borehole B4, the elevated water-level in the pond-shore would lead less positive heat flux down to underlying permafrost because of higher thermal capacity, while more thermal energy could be released from underlying permafrost during freezing period because of smaller thermal capacity. This contrast impacts can significantly influence the annual net energy flux. However, the thinner permafrost close to the pondshore might be related to bottom lateral warming effect of the open talik. In general, lateral thermoerosion of the pond by heat conduction is rather weak compared to the vertical thermoerosion.

5 Discussions

5.1 Influence of measurement technique

In this study, the net lateral flux was calculated from the water balance with other three measured or estimated components. As a result, its accuracy is strongly related to the accuracy of them. Generally, the small uncertainty of the pond water-level measurement is within 5 mm, but the daily rainfall estimated from the soil moisture measurements and the estimated evaporation would be much higher. However, compared to the large quantity of the calculated net lateral flux, these uncertainties cannot mask the significant role of the net lateral flux. Based on those measurements, we are allowed to qualitatively interpret the hydrological regime of the ponds. This would extend our understanding of the shallow thermokarst ponds on the QTP.

5.2 Implications for studying thermal evolution of shallow thermokarst ponds on the QTP

Along with climate warming, permafrost degradation is characterized as rising temperature and thickening active layer. As a result, thermokarst pond expansion would be ex-

pected as found by Jones et al. (2011) in continuous permafrost regions, Alaska. However, for the topography-controlled thermokarst deepening active layer is not doomed to an expanding pond, reversely it might shrink. In addition, the factor of changing precipitation would be also important for the rainwater-dominated thermokarst ponds on the QTP. The variation of pond water area is strongly related to the monsoon-driven precipitation. Observations in this study demonstrate that, compared to the abrupt increase of rainwater recharge over half a meter, the contribution of the melting water of the thawing permafrost with a rate of a few centimeters per year is trivial. Even in flat lowlands with inhibited drainage it would be still challenging to relate the change of pond water area of the rainwater-dominated thermokarst ponds to permafrost degradation at a decadal-scale on the QTP. Particularly, precipitation observed from the weather stations in this region from 1962 to 2004 show an increasing trend (Li et al., 2006).

Considering the significant role of hydrological regime in the development of rainwater-dominated thermokarst ponds, the specific hydrological processes had better be considered in modeling thermokarst ponds on the QTP. First, the trend of precipitation and its variability is essential to pond water-level dynamics. Since the heavy rainfall could lead significant changes of pond water-level, detailed precipitation information from climate simulations would be very helpful in predict thermokarst pond development. Particularly, expansion or shrink of pond water can significantly change the vertical balance at pondshore, and this would be essential to understand quick retreat of lakeshore (e.g. Lin et al., 2010). Second, subsurface lateral flow surrounding the ponds plays an important role in the pond shape and future development by lateral thermoerosion. The thermoerosion mechanism of the shallow thermokarst ponds is closely related to the rainwater-controlled hydrological regime, its pace would be influenced by the inter-annual variability of rainfall. This is different from the thermoerosion mechanism of thermokarst lakes in other environments. For instance, studies in the pan-Arctic regions demonstrate that lateral thermal erosion can take place at the shores of ponds with significant wave activity and its erosion direction is controlled by wind direction (Jones et al., 2011). Another example is significant surface water

flow caused thermoerosional gullies in ice-rich lowlands with sufficient relief gradients (e.g. Fortier et al., 2007; Godin and Fortier, 2012).

6 Conclusions

This study provides some insights of hydrological and thermal regimes of shallow thermokarst ponds on the northeastern QTP, and some implications for studying thermoerosion of this kind of thermokarst ponds. Generally conclusions are summarized as follows.

1. Controlling by the summer monsoon on the northeastern QTP, annual variability of thermokarst pond water-level regime is dominated by rainfall. Generally, pond water-level regime experiences a slightly decrease during pre-rainy season, abrupt elevated rise during the rainy season, a gradual declining during the post rainy season till complete frozen of surrounding active layer.

2. Apart from temporal stream flow, subsurface lateral flow plays a dominant role in the interaction between pond water and surrounding active layer. Depending on the amount and intensity of rainfall, annual fluctuation of pond water-level can vary greatly at different ponds. In contrary, the role of deepening active layer led by permafrost degradation would expect to be quite weak in yearly scale. Therefore, water areal change of shallow thermokarst ponds on the northeastern QTP is more related to annual variation of rainfall.

3. The rainwater induced fluctuation of pond water-level leads significant annual variation in pond thermal regime. Another notable feature is extraordinary warming during the late ice-cover period that evident air gap between upper ice-cover and underlying water, led by upward thawing of ice-cover, results in greenhouse-like condition due to the unique weather that strong radiation and little snowpack.

The hydrological mechanism influences thermal regime and thermoerosion of the shallow thermokarst ponds. For a long time-scale, the trend of precipitation and associated hydrological regime would be essential to simulate thermal evolution of shallow thermokarst ponds on the QTP.

Acknowledgements. We would like to thank Lei Guo and Xinbing Wang for field assistance. This research was funded by the National Natural Science Foundation of China (Grant No. 41171059).

References

Allen, R. G., Pereira, L. S., Raes, D., and Smith, M.: Crop Evapotranspiration – Guidelines for Computing Crop Water Requirements, FAO Irrigation and Drainage Paper 56, United Nations Food and Agriculture Organization, Rome, Italy, 1998.

Bowling, L. C., Kane, D. L., Gieck, R. E., Hinzman, L. D., and Lettenmaier, D. P.: The role of surface storage in a low-gradient Arctic watershed, Water Resour. Res., 39, 1087, doi:10.1029/2002WR001466, 2003.

Brocca, L., Moramarco, T., Melone, F., and Wagner, W.: A new method for rainfall estimation through soil moisture observations, Geophys. Res. Lett., 40, 853–858, doi:10.1002/grl.50173, 2013.

Famiglietti, J. S. and Wood, E. F.: Multiscale modeling of spatially variable water and energy balance processes, Water Resour. Res., 11, 3061–3078, 1994.

Finch, J. and Calver, A.: Methods for the Quantification of Evaporation from Lakes, World Meteorological Organization Commission of Hydrology, CEH Wallingford, UK, 2008.

Fortier, D., Allard, M., and Shur, Y.: Observation of rapid drainage system development by thermal erosion of ice wedges on Bylot Island, Canadian Arctic Archipelago, Permafrost Periglac., 18, 229–243, doi:10.1002/ppp.595, 2007.

Godin, E. and Fortier, D.: Fine-Scale Spatio-Temporal Monitoring of Multiple Thermoerosion Gully Development on Bylot Island, Eastern Canadian Archipelago, Tenth International Conference on Permafrost, vol. 1, International Contributions, The Northern Publisher, Salekhard, Russia, 125–130, 2012.

Grosse, G., Jones, B., and Arp, C.: Thermokarst lakes, drainage, and drained basins, in: Treatise on Geomorphology, vol. 8, Glacial and Periglacial Geomorphology, Academic Press, San Diego, USA, 325–353, 2013.

Harris, S. A.: Causes and consequences of rapid thermokarst development in permafrost or glacial terrain, Permafrost Periglac., 13, 237–242, 2002.

Hayashi, M. and van der Kamp, G.: Water level changes in ponds and lakes: the hydrological processes, in: Plant Disturbance Ecology, Academic, San Diego, USA, 311–339, 2007.

Hinkel, K. M., Jones, B. M., Eisner, W. R., Cuomo, C. J., Beck, R. A., and Frohn, R.: Methods to assess natural and anthropogenic thaw lake drainage on the western Arctic coastal plain of northern Alaska, J. Geophys. Res., 112, F02S16, doi:10.1029/2006JF000584, 2007.

Jones, B. M., Grosse, G., Arp, C. D., Jones, M. C., Walter Anthony, K. M., and Romanovsky, V. E.: Modern thermokarst lake dynamics in the continuous permafrost zone, northern Seward Peninsula, Alaska, J. Geophys. Res., 116, G00M03, doi:10.1029/2011JG001666, 2011.

Kääb, A. and Haeberli, W.: Evolution of a high-mountain thermokarst lake in the Swiss Alps, Arct. Antarct. Alp. Res., 33, 385–390, 2001.

Li, L., Li, F., Guo, A., and Zhu, X.: Study on the climate change trend and its catastrophe over "Sanjiangyuan" region in recent 43 years, J. Nat. Resour., 21, 79–85, 2006.

Li, S., Zhan, H., Lai, Y., Sun, Z., and Pei, W.: The coupled moisture–heat process of permafrost around a thermokarst pond in Qinghai–Tibet Plateau under global warming, J. Geophys. Res.-Earth, 119, 836–853, doi:10.1002/2013JF002930, 2014.

Lin, Z., Niu, F., Xu, Z., Xu, J., and Wang, P.: Thermal regime of a thermokarst lake and its influence on permafrost, Beiluhe basin, Qinghai–Tibet Plateau, Permafrost Periglac., 21, 315–324, doi:10.1002/ppp.692, 2010.

Lin, Z., Niu, F., Liu, H., and Liu, J.: Hydrothermal processes of Alphine Tundera Lakes, Beiluhe Basin, Qinghai–Tibet Plateau, Cold Reg. Sci. Technol., 65, 446–455, 2011.

Lin, Z., Niu, F., Liu, H., Lu, J., and Luo, J.: Numerical simulation of lateral thermal process of a thaw lake and its influence on permafrost engineering on Qinghai–Tibet Plateau, Chinese J. Geotech. Eng., 34, 1394–1402, 2012.

Ma, Y., Yao, T., and Wang, J.: Experimental study of energy and water cycle in Tibetan Plateau – the progress introduction on the study of GAME/Tibet and CAMP/Tibet, Plateau Meteorol.„ 25, 344–351, 2006.

Mackay, J. R.: Lake stability in an ice-rich permafrost environment: examples from the western Arctic coast, in: Aquatic Ecosystems in Semi-Arid Regions: Implications for Resource Management, NHRI Symposium Series 7, Environment Canada, Saskatoon, Canada, 1–26, 1992.

Marsh, P., Russell, M., Pohl, S., Haywood, H., and Onclin, C.: Changes in thaw lake drainage in the western Canadian arctic from 1950 to 2000, Hydrol. Process., 23, 145–158, 2009.

Monteith, J.: Evaporation and the Environment, 19th Symposium of the Society of Experimental Biology, Cambridge University Press, Cambridge, 205–234, 1965.

Morgenstern, A., Günther, F., Ulrich, M., Fedorova, I., Rudaya, N., Boike, J., and Schirrmeister, L.: Evolution of thermokarst lakes and alasses in the ice-rich permafrost of the Lena River Delta, Russian–German cooperation in the scientific exploration of northern Eurasia and the adjacent Arctic ocean, Leopoldina Symposium in cooperation with St. Petersburg State University and the Russian Academy of Sciences, 10–12 September 2012, St. Petersburg, 2012.

Niu, F., Lin, Z., Liu, H., and Lu, J.: Characteristics of thermokarst lakes and their influence on permafrost in Qinghai–Tibet Plateau, Geomorphology, 132, 222–233, 2011.

Pan, X., You, Y., Roth, K., Guo, L., Wang, X., and Yu, Q.: Mapping permafrost features that influence the hydrological processes of a thermokarst lake on the Qinghai–Tibet Plateau, China, Permafrost Periglac., 25, 60–68, doi:10.1002/ppp.1797, 2014.

Pohl, S., Marsh, P., and Bonsal, B. R.: Modeling the impact of climate change on runoff and annual water balance of an arctic headwater basin, Arctic, 60, 173–186, 2007.

Pohl, S., Marsh, P., Onclin, C., and Russell, M.: The summer hydrology of a small upland tundra thaw lake: implications to lake drainage, Hydrol. Process., 23, 2536–2546, 2009.

Smith, L. C., Sheng, Y., and MacDonald, G. M.: A first pan-Arctic assessment of the influence of glaciation, permafrost, topography and peatlands on Northern Hemisphere lake distribution, Permafrost Periglac., 18, 201–208, 2007.

Turner, K. W., Wolfe, B. B., and Edwards, T. W. D.: Characterizing the role of hydrological processes on lake water balances in the Old Crow Flats, Yukon Territory, Canada, using water isotope tracers, J. Hydrol., 386, 103–117, 2010.

van Everdingen, R. O.: Multi-language glossary of permafrost and related ground-ice terms, National Snow and Ice Data Center, Boulder, CO, 1998.

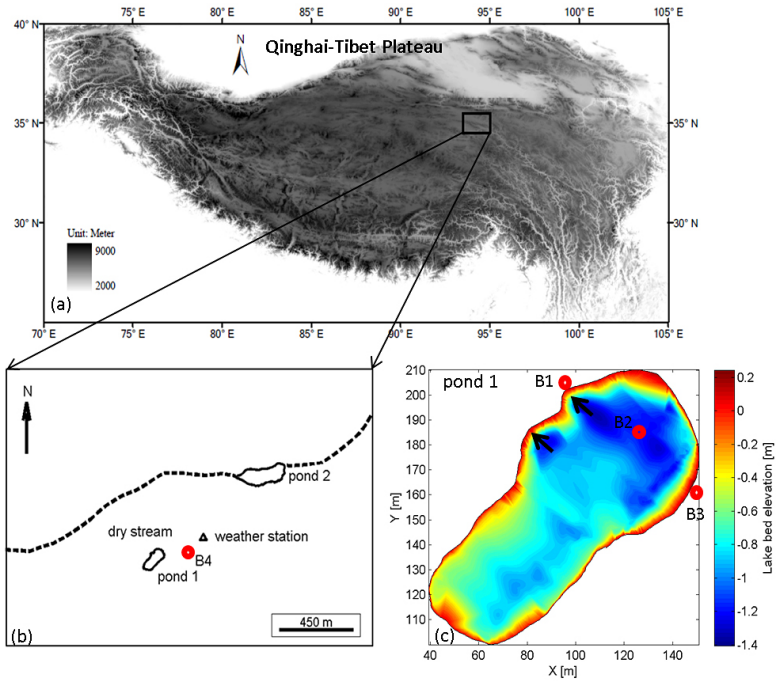

Figure 1. Location of two ponds and instrumentation at the study site. **(a)** Topography of the Qinghai–Tibet Plateau. **(b)** Soil–weather monitoring station and a deep borehole (B4). **(c)** Pond bed topography and shape of Pond 1 (modified from Pan et al., 2014) and three borehole locations (B1, B2 and B3). Two arrows show the preferential erosion.

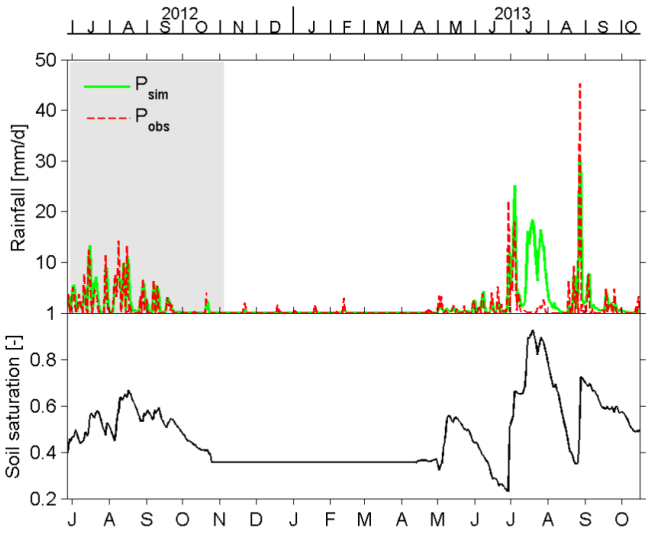

Figure 2. Comparison of observed and simulated daily rainfall and in-situ soil water content measurements.

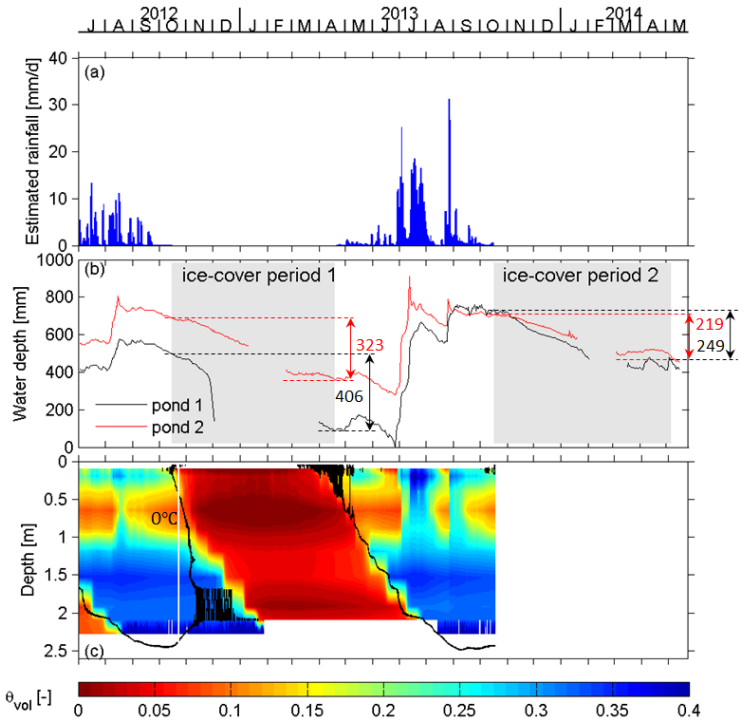

Figure 3. Response of pond water storage to precipitation and freeze and thaw of adjacent active layer during the period from July 2012 to May 2014. **(a)** Rainfall excluding solid precipitation. **(b)** Pond water dynamics in the Pond 1 and the Pond 2; dashed lines show the drop of water-level during ice-cover periods. **(c)** Soil water dynamics and thawing front (black curve) in the monitoring profile at the weather station (Fig. 1b). θ_{vol}: volumetric water content.

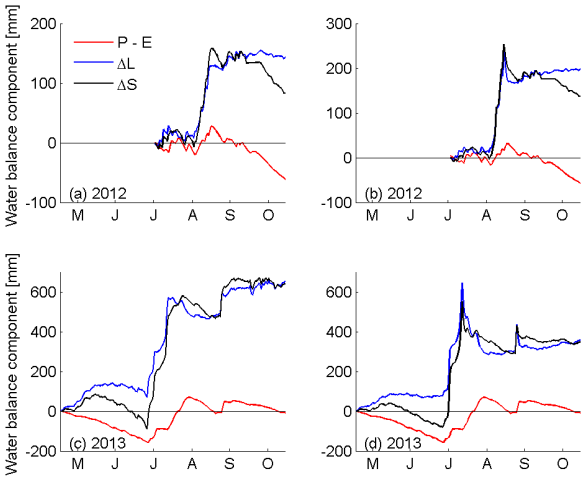

Figure 4. Significant role of lateral flow in water budget of two ponds in 2012 and 2013. Pond 1: **(a)** and **(c)**; Pond 2: **(b)** and **(d)**. $P - E$: accumulative net rainfall; ΔL: accumulative net lateral flux; ΔS: water level.

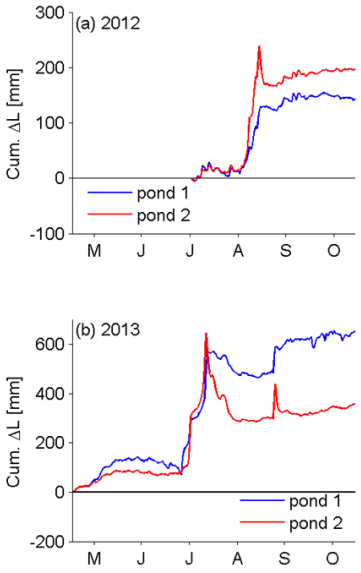

Figure 5. Different responses of net lateral flux at Pond 1 and Pond 2 in the years of 2012 and 2013. **(a)** Bigger accumulative net lateral flux at Pond 2 in the dry year. **(b)** Smaller accumulative net lateral flux at Pond 2.

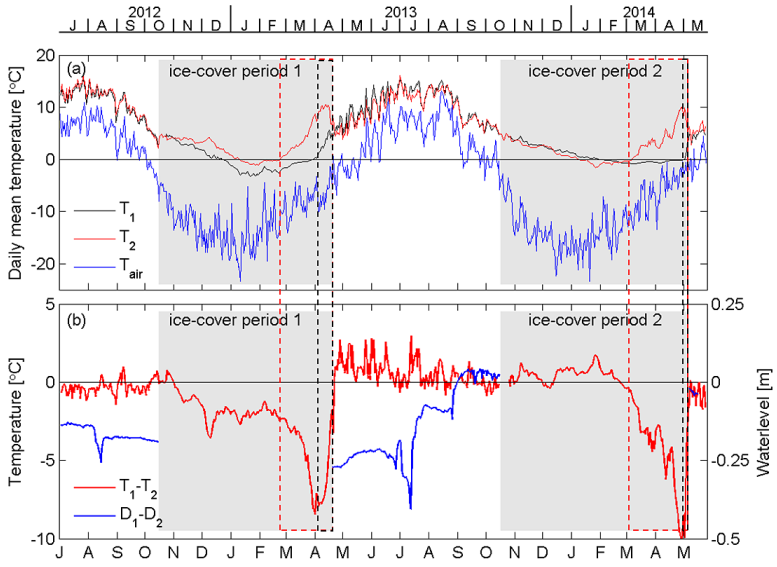

Figure 6. Influences of seasonal fluctuation of pond water-level on pond bottom thermal regime during ice-cover period. **(a)** Fluctuation of pond bottom temperature (T_1 and T_2) at Pond 1 and Pond 2 and air temperature (T_{air}). **(b)** Relation between pond bottom temperature difference and pond water-level difference (D_1 and D_2) of the two ponds. Black and red dashed boxes show bottom thawing periods for Pond 1 and Pond 2, respectively.

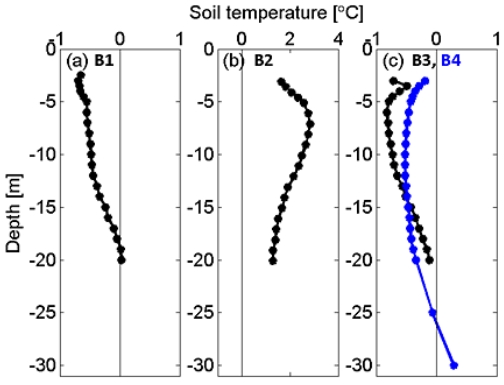

Figure 7. Ground temperatures measured from boreholes at different locations (Fig. 1) in 2014.